Rain in Shallow and Deep Convection Measured with a Polarimetric Radar

ALEXANDER V. RYZHKOV

Cooperative Institute for Mesoscale Meteorological Studies, University of Oklahoma, Norman, Oklahoma

DUSAN S. ZRNIĆ

NOAA, National Severe Storms Laboratory, Norman, Oklahoma

(Manuscript received 22 December 1995, in final form 11 April 1996)

ABSTRACT

The authors contrast rainfall in two Oklahoma squall lines: one with deep convection occurred in the spring and the other with shallower convection in the winter. Both passed over a micronetwork of densely spaced rain gauges and were observed with the National Severe Storm Laboratory's polarimetric weather radar. Polarimetric measurements reveal differences in storm structure that in turn imply that microphysical processes caused the drop size distributions to be quite distinct for the two events. In the winter squall line the conventional $R(Z)$ algorithm for estimating rainfall fails badly, whereas in the summer squall line it performs well. The method based on specific differential phase measurements, however, yields a very good match between radar-derived areal precipitation amount and rain depth obtained from the micronetwork of densely located rain gauges for both events.

1. Introduction

Variations in drop size distribution (DSD) can cause significant errors in radar rainfall estimates if a rain rate–reflectivity factor $R(Z)$ relation is used. It has been established that even during a single rain event DSD can change considerably and one needs to use appropriate $R(Z)$ relations for different stages of the storm (Dingle and Hardy 1962; Carbone and Nelson 1978) to account for these variations. Some argue (Rosenfeld et al. 1995) that Z and R should be matched in probability according to storm type, structure, and distance from the radar. Although such matching lessens the effects of DSD variability, there are other sources of error to which Z is prone. These are radar calibration errors, attenuation, hail contamination, partial beam blocking, and use of ground clutter cancelers (Zrnić and Ryzhkov 1996). Radar estimates of rain derived from the specific differential phase K_{DP} measurements are less sensitive to DSD variations and are less affected by the other artifacts (Sachidananda and Zrnić 1987; Ryzhkov and Zrnić 1995b; Zrnić and Ryzhkov 1996).

There is much literature on DSDs and conditions associated with equilibrium drop spectra or the lack thereof (e.g., Carbone and Nelson 1978; Willis 1994; Hu and Srivastava 1995). The subject is particularly complex in a continental convective system with significant ice phase processes [see the correspondence between Carbone (1985) and Willis (1985)]. Initial conditions of hail or graupel sizes (which melt to produce rain) and strength of convection (updrafts) influences the evolution of DSD so that it can seldom reach equilibrium. In principle it is possible to envision a steady distribution of drop and hail sizes at a given height if the input hail sizes above the melting layer do not change. There are no observations or models that adequately address this issue. Nevertheless, the radar variables are derived from weighted averages of such distributions, and it is these variables that are used for estimating rainfall on the ground. Thus, for agreement between gauges and radar measurements the assumed distribution used to relate the rain rate to the radar variables should be representative of the distribution near the ground.

In this paper we contrast rainfall in two Oklahoma squall lines, one of which occurred in the spring the other in the winter. Both passed over a micronetwork of densely spaced rain gauges and were observed with the National Severe Storm Laboratory's polarimetric weather radar. Polarimetric measurements reveal differences in storm structure that in turn imply that microphysical processes caused the DSD to be quite distinct for the two events.

We illustrate the performance of a polarimetric rainfall estimator in the case of the winter squall line, for which the conventional $R(Z)$ algorithm fails badly. This is in contrast to the summer squall line, for which

Corresponding author address: Dr. Dusan Zrnić, National Severe Storms Laboratory, 1313 Halley Circle, Norman, Oklahoma 73069.

the $R(Z)$ algorithm performs well. The method based on K_{DP} measurements, however, yields a very good match between radar-derived areal precipitation amount and rain depth obtained from the micronetwork of densely located rain gauges for both events.

We explore the causes leading to the failure of the $R(Z)$ algorithm using simple model considerations and the structure of precipitation in the storm.

2. Description of the winter case

In the afternoon of 19 February 1994 a squall line passed over a 50 km × 40 km radar test area where 42 rain gauges are located (Fig. 1). These gauges constitute the Little Washita River watershed network, which is maintained by the Agricultural Research Service. In the middle of the observation period, the squall line was oriented northeast to southwest within the test area (Fig. 2a). The line propagated to the east with an average speed of 50 km h^{-1}. According to National Climatic Data Center (1994) data this squall line produced hail with a diameter of up to 1 inch on the ground east of the test area. No hail was reported in the test area during the passage of the squall line.

One-hour gauge accumulations for each gauge were obtained for the period (between 2100 and 2200 UTC) that the line was over the network. To make radar and gauge data compatible, we interpolated rain accumulations from gauges to the basin area (i.e., test area) defined by the gauges at the perimeter. The resulting rain depth field is shown in Fig. 3a. Mean rain rate $\langle R \rangle$ for this area was estimated as 1-h areal accumulation divided by the watershed area; for this storm $\langle R \rangle$ is 11.7 mm h^{-1}.

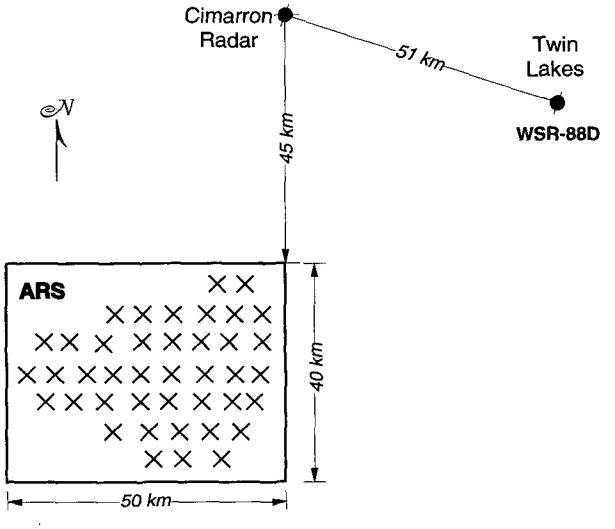

FIG. 1. Location of the polarimetric radar, the WSR-88D radar, and the Little Washita rain gauge network.

Radar-derived rain depths and corresponding *mean* rain rates were obtained using the conventional Marshall–Palmer (MP) relation,

$$Z = 200R^{1.6}, \tag{1}$$

and a polarimetric algorithm based on K_{DP} measurements. Radar data from the elevation scan of 0.5° were processed, which had an update time of about 3.5 min.

To reduce the effects of statistical errors, we have adapted the polarimetric rainfall estimator

$$R = 40.6K_{DP}^{0.866} \tag{2}$$

from Sachidananda and Zrnić (1987) as follows. We separate light from heavy rainfall with a 40-dBZ reflectivity threshold. In areas of light rain we use an averaging scale for differential phase data that is three times larger than in areas of heavier rainfall.

The Marshall–Palmer $R(Z)$ relation yields a mean rain rate of 4.3 mm h^{-1} that is only one-third that of the gauge measurements. This is in contrast to the polarimetrically derived mean areal rain rate $\langle R \rangle$ = 10.9 mm h^{-1}, which is in good agreement with the gauges. The scattergrams of rain accumulations obtained by radar and gauges (Fig. 4) illustrate the performance of the $R(Z)$ and $R(K_{DP})$ estimators. To check Cimarron radar calibration, we have estimated the rain depth over the same area using the nearby Twin Lakes WSR-88D radar (Fig. 1). The $R(Z)$ algorithm (1) was applied to WSR-88D data, and it produced a mean rain rate of 4.7 mm h^{-1}; this is nearly identical to the result obtained when using Z from the Cimarron radar. Clearly, calibration is not a likely cause of the large underestimates produced by the Marshall–Palmer relation. A slightly different $R(Z)$ relation, $Z = 300R^{1.4}$, employed in the WSR-88D rainfall algorithm, gave a very similar result, $\langle R \rangle$ = 4.6 mm h^{-1}.

Consistency between the two radar measurements of reflectivity and their significant departure from polarimetric and gauge estimates prompted a careful examination of the data. The rain depth fields obtained from the Cimarron and WSR-88D radars are represented in Figs. 3b–d. Note a good agreement of the spatial structure in all three fields, although the fields derived from the reflectivity factor contain considerably less rainfall. The main features of the fields obtained from the specific differential phase (Fig. 3c) and rain gauges (Fig. 3a) agree. Nevertheless, even this relatively dense gauge network misses important details of the rainfall depth structure, such as the tracks of individual cells. The gauge spacing (about 5 km) is too coarse to capture the fine details of the precipitation pattern. The radar field has a resolution of about 1 km, which is also its sampling interval; thus, it represents well the dominant spatial structure (wavelength of about 6–8 km) in the northwest to southeast direction. In the rain gauge field this structure is spatially aliased and then smoothed by interpolation.

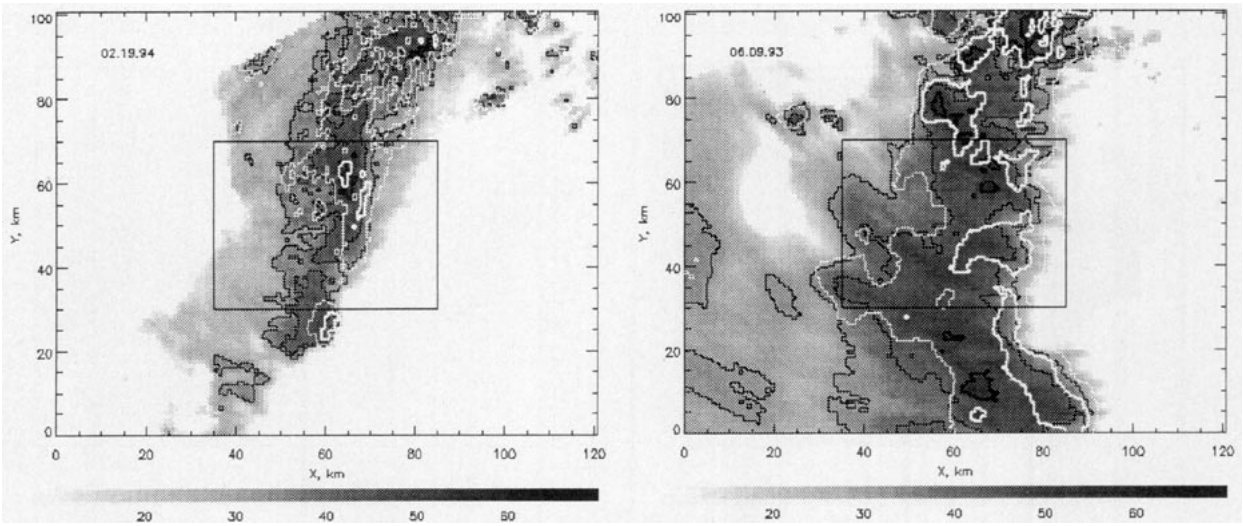

FIG. 2. The location of the squall line with respect to the rain gauge area on (a) 19 February 1994 and (b) 9 June 1993. The rain gauge area is outlined by the rectangle. Gray shades and black contours indicate Z, and superimposed white contours represent Z_{DR}; Z contours are drawn every 10 dBZ starting from 30 dBZ. The thin Z_{DR} contour corresponds to 1 dB, and the thick Z_{DR} contour corresponds to 2 dB.

3. Interpretation of the data

To understand the failure of the Marshall–Palmer relation, we compare this case with a typical spring/summer mesoscale convective system. We chose the squall line of 9 June 1993 in which both $R(Z)$ and $R(K_{DP})$ estimates agree well with rain depth measured by the gauges. Although we have good agreement between $R(Z)$ and $R(K_{DP})$ in other systems, the June system is convenient because much of the analysis has been performed (Ryzhkov and Zrnić 1995a,b). The June squall line was oriented north–south (Fig. 2b), whereas the February line had a southwest–northeast orientation. Both lines propagated eastward, and the June storm produced some hail on the ground in the northwestern corner of the test area at the beginning of the observation period. Maximum reflectivity in the test area at the elevation of 0.5° was 57.2 dBZ for the February case and 63.5 dBZ for the June case. In spite of higher reflectivity and larger size the June squall line generated lower hourly rain accumulation rates ($\langle R \rangle = 10.7$ mm h^{-1}) over the test area than the February line.

Of crucial importance to our interpretation is that the rainfall measurements on both days, based on $R(K_{DP})$ at 500 m above ground, agree with the gauges. Thus, the DSD evolution from that height to the ground is presumed not significant and unlikely to explain the inadequacy of the $R(Z)$ estimator in the February case. We hypothesize that the February storm had a drop size distribution with a deficit of large raindrops but high concentration of smaller drops, whereas in the June storm the DSD had a substantial amount of large drops. We submit that the raindrop size distribution near the ground is influenced by the size and composition of solid hydrometeors aloft (Carbone 1985). It appears that melting is the dominant factor in shaping the DSD. To substantiate these hypotheses, we present polarimetric radar data next.

In Fig. 5 are the vertical profiles of radar reflectivity factor Z, differential reflectivity Z_{DR}, and specific differential phase K_{DP} in the major reflectivity core of the February and June storms at the time the core was centered on the gauge network. The June storm had a height of 14–15 km, whereas the February storm was relatively shallow with a top of only 8 km. Reflectivity factors at all heights in the summer storm exceed the reflectivity factors at the corresponding heights in the winter storm. The 30-dBZ contour reaches 10 km in the June storm, but is barely 5 km high in the February storm. Furthermore, in this storm the height of the 45-dBZ contour is at only 3 km. Clearly, the June storm had a much more vigorous updraft, over 25 m s^{-1} estimated from the radial divergence, which had a maximum of over 4×10^{-3} s^{-1} at a height of 13.5 km in one strong cell. Maximum divergence in the February storm was 5×10^{-4} s^{-1} at a height of 7.5 km. The divergence of 4×10^{-3} s^{-1} was almost constant over 10 km in the horizontal direction (June storm) and thus likely to indicate the presence of 2.5-cm diameter hailstones (Witt and Nelson 1991). This is also in accord with the criterion proposed by Waldvogel et al. (1979) that states that hail is probable if the 45-dBZ contour is 1.4 km above the 0°C level. In June the environmental zero degree isotherm was at 4 km and in February it was at 3.5 km. Hence, it follows from the profiles in Fig. 5 that the June storm was likely to produce hail and the February storm was not. Therefore, in the latter case it is natural to expect smaller sizes of solid hydrometeors aloft and, as a result, narrower DSD near the ground.

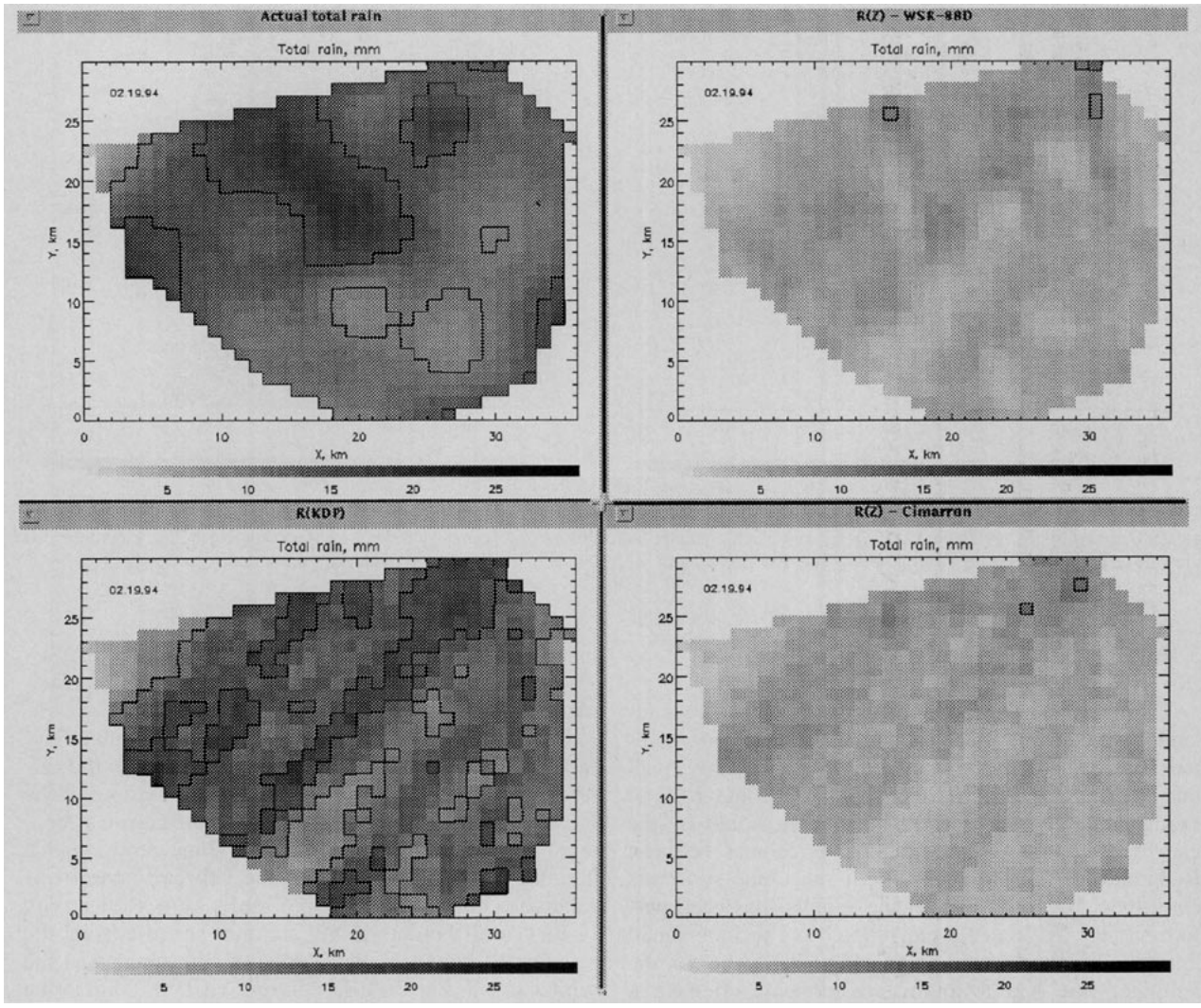

FIG. 3. A 1-h rain depth map in the rain gauge area obtained (a) from the gauges, (b) from the WSR-88D using $R(Z)$, (c) from the polarimetric radar using $R(K_{DP})$, and (d) from the polarimetric radar using $R(Z)$.

The bulk properties of falling hydrometeors are captured in the K_{DP} and Z_{DR} profiles (Fig. 5). The increase of K_{DP} indicates melting (Balakrishnan and Zrnić 1990), which in the June case starts at about 3 and ends at 1.5 km, and in the February case it starts at 2.5 and ends at 1 km (Fig. 5). The onset of melting at lower altitudes from the environmental zero isotherm is most likely caused by the downdrafts and cooling due to melting. We believe that the difference of 500 m in the location of the melting zone is not sufficient to explain the difference in the two DSDs for the following reasons. First, thicknesses of the melting zones are about equal; therefore, the melting process for similar particles should be similar. Evidently at the bottom of the melting zone the DSDs are different because the hydrometeor population at the top of the melting zones differ. Second, for the February case the bottom of the melting zone is 500 m above the location of the radar resolution volume (elevation 0.5°) and it is 1000 m for the June case (Fig. 6), yet the $R(K_{DP})$ estimates agree with the rain gauges. Thus, the 500-m longer path to the ground could make a difference in the evolution of the June DSD. We argue that this is unlikely. Assuming that coalescence and breakup are dominant evolution mechanisms, Srivastava (1971) found that for a liquid water content of 1 g m^{-3} (reflectivity factor of about 47 dBZ) the time to reach equilibrium is 1500 s. Hu and Srivastava (1995) used a more sophisticated model to predict that for a rainfall rate of about 50 mm h^{-1} the equilibrium shape is attained in a fall of about 2 km in 10–15 min. Both times are considerably longer than the time (less than 100 s) it would take for the drops in still air to descend 500

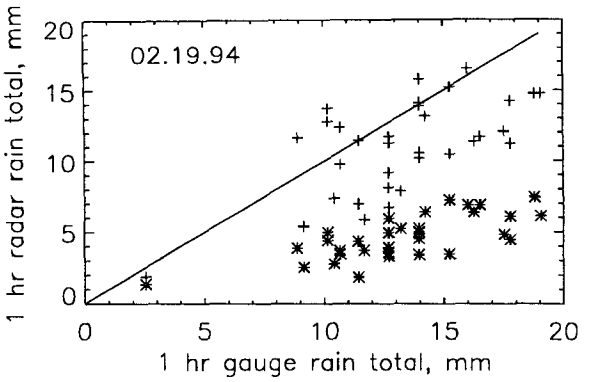

FIG. 4. Rain accumulations obtained by radar and rain gauges for the 19 February 1994 case. The symbol asterix stands for the Marshal–Palmer $R(Z)$ relation and the cross represents the $R(K_{DP})$ relation.

m. Because heavy rain is imbedded in downdrafts, the time to descend would be even shorter.

In summary we considered two factors that could favor wider DSD for the June case: 1) the bottom of the melting zone is higher, and consequently raindrops have more time to grow through coalescence; and 2) the initial size distribution of frozen particles aloft in the June case is much wider, which results in an abundance of large raindrops at the bottom of the melting zone. But physical considerations in the previous paragraph eliminate factor 1), and hence we are left with factor 2).

Note that the K_{DP} near the ground is significantly larger for the February storm, whereas Z_{DR} is larger for the June storm (Fig. 5). The maximum K_{DP} registered elsewhere on 19 February 1994 is 6.4° km^{-1} compared to 4.5° km^{-1} observed on 9 June 1993. This is a strong argument in favor of our hypothesis that the February rain is composed of smaller raindrops in very high concentration. Briefly, the physical explanation of the measurement is as follows. Z_{DR} is a measure of the volume-weighted axis ratio of drops and is proportional to the median drop size (Jameson 1983). Thus, larger Z_{DR} implies the presence of larger drops. K_{DP} is proportional to drop concentration and size. Therefore, in the February case the concentration must be higher than in the June case to explain the larger K_{DP}.

The relative values of Z_{DR} and K_{DP} in the two events just discussed were observed not only in the middle of the strongest reflectivity cell but also elsewhere in the storm. On average Z_{DR} in Fig. 2a is lower than in Fig. 2b, implying that raindrops are smaller in the February squall line. Extended areas with $Z_{DR} > 2$ dB at the leading edge of the June squall line mark the regions of strong updraft in which low concentration of large drops might be due to gravitational and wind shear sorting (Bringi et al. 1991). There is only a slight hint that a similar effect is present in the February case.

To make a better quantitative assessment of drop sizes, we have analyzed the relations between K_{DP}, Z, and Z_{DR} for both storms during the whole observation period. The average values of Z and Z_{DR} were computed for K_{DP} in the intervals of 0.2° km^{-1} and centered at 1, 1.5, 2, 2.5, and 3° km^{-1} (Fig. 7). In Fig. 7 the bias in the reflectivity factor ΔZ caused by attenuation has been accounted for by using the formula (Bringi et al. 1990)

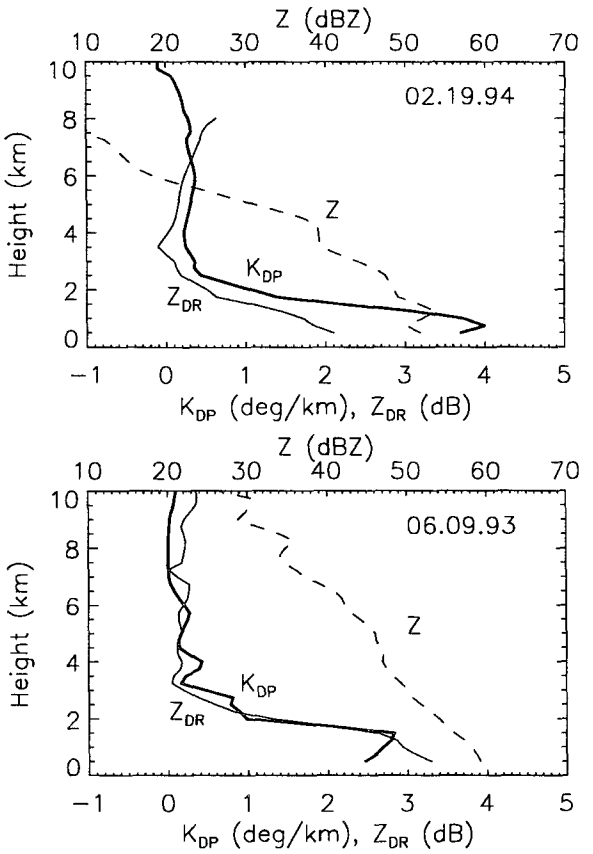

FIG. 5. Vertical profiles of radar variables in the major reflectivity core (a) on 19 February 1994 and (b) on 9 June 1993.

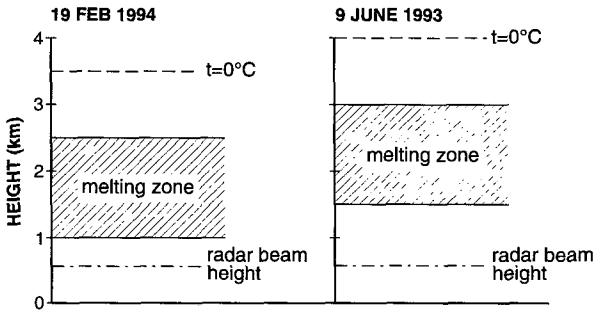

FIG. 6. Heights of the zero degree isotherm, the melting zone, and the radar resolution volume during the storms of 9 June 1993 and 19 February 1994.

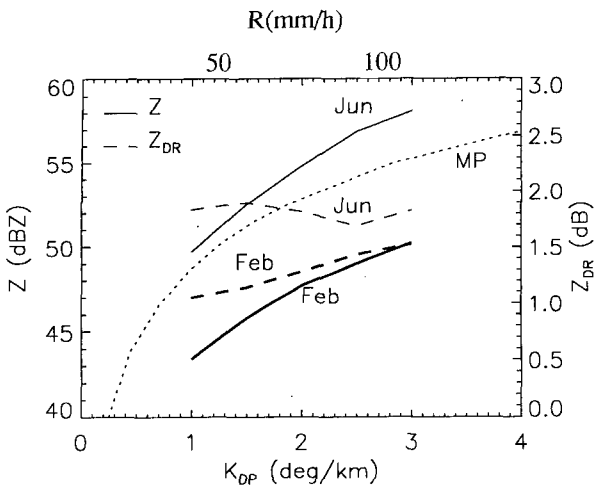

FIG. 7. Average Z and Z_{DR} at 0.5° elevation and in the rain gauge network area as a function of K_{DP} for the June and February storms. The dotted curve represents the relation between K_{DP} and Z for the MP drop size distribution.

$$\Delta Z = -a\Phi_{DP}, \tag{3}$$

where Φ_{DP} is the total differential phase.

A similar formula exists for correcting differential reflectivity errors caused by differential attenuation:

$$\Delta Z_{DR} = -b\Phi_{DP}. \tag{4}$$

The maximum value of Φ_{DP} in the test area is 181° for the June storm and 215° for the February storm. The coefficients a and b depend on the DSD, possible presence of melting hail, and temperature (Jameson 1992; Ryzhkov and Zrnić 1995b). The theoretical estimates of a and b are about 0.02 dB deg^{-1} and 0.0035 dB deg^{-1}, respectively, for the DSD close to the Marshall–Palmer distribution (Bringi et al. 1990; Jameson 1992). Experimentally obtained a was 0.036 dB deg^{-1} in the test area for the June storm; this is almost twice the value (0.021 dB deg^{-1}) found for the February storm. We have made the appropriate corrections for Z using these estimates of a.

Examination of differential reflectivity data suggests that some differential attenuation might have been present on both days. Because of large uncertainty we have not accounted for this possible bias in Fig. 7.

Note that the reflectivity factor values for the June storm cell exceed by 6–8 dB the values for the February cell at the same values of K_{DP}. Furthermore, the $Z(K_{DP})$ curve for the June storm is much closer to the curve valid for the Marshall–Palmer distribution (MP truncated at a maximum diameter of 8 mm) than the curve for February. The larger departure from the MP curve (June case) at higher reflectivities is likely caused by the presence of hail.

The Z_{DR} curve in the February case is increasing with the increase of K_{DP} but is nearly constant in the June case; furthermore, it is larger for the June storm. This suggests that the rates of binary processes (collision coalescence and breakup) and spontaneous breakup at the very large drop end of the spectrum for the June case do not seem to be changing the concentrations of the large drops very rapidly during sedimentation. Thus, the large drops are nearly independent of rain rate in the June storm. Another reason for high concentration of large drops could be the presence of melting hail, which provides input at larger sizes. Melting ice cores in the drops prevent spontaneous breakup. Although the median drop size increases slightly with the rain rate in the February rain, the size is always smaller than the corresponding size of the June drops.

Next we estimate the size of raindrops that contribute most to the observed radar parameters. For this purpose we examine the ratio K_{DP}/Z (Z is in mm^6 m^{-3}) and differential reflectivity Z_{DR} as a function of raindrop equivolume diameter (i.e., diameter of a sphere with the same volume as the raindrop) for a monodisperse drop size distribution. Both quantities are independent of the concentration but depend on the size of raindrops. Figure 8 illustrates these dependencies computed for the axis ratio

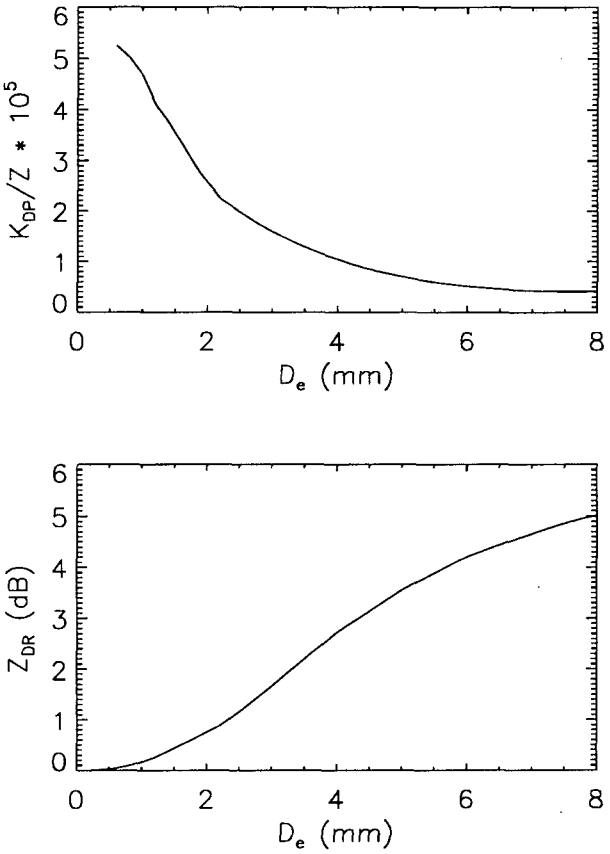

FIG. 8. The dependence of the ratio (a) K_{DP}/Z and (b) Z_{DR} on the raindrop equivolume diameter for the monodisperse raindrop distribution at the wavelength of 10.97 cm.

versus size specified by Pruppacher and Pitter (1971). The observed range of the K_{DP}/Z ratio is (0.5–1.1) 10^{-5} (deg km^{-1})/(mm^6 m^{-3}) for the June case, and the corresponding range for the winter squall line is (2.6–4.3) 10^{-5} (deg km^{-1})/(mm^6 m^{-3}). According to Fig. 8a, the K_{DP}/Z values for the summer event correspond to $D_e > 4$ mm, whereas the range of the K_{DP}/Z ratio for the winter squall line fits the narrow interval of drop diameters between 1 and 2 mm. Measured Z_{DR} data (Fig. 7) in the June storm correspond to $D_e > 3$ mm (Fig. 8). Observed Z_{DR}s in the winter storm (Fig. 7) are somewhat larger (by 0.5–1 dB) than expected for the raindrops with diameters between 1 and 2 mm (see Fig. 8b). A possible reason for this might be that the monodisperse model is not adequate and/or the differential reflectivity is heavily weighted by large drops—even more than the reflectivity factor. Therefore, very few big drops added to the abundance of small drops with diameters between 1 and 2 mm increase Z_{DR} appreciably but do not much affect the ratio K_{DP}/Z. In any case our analysis points out that there is a paucity of large drops in the February case compared to the June case.

4. Conclusions

We have examined rainfall in a winter squall line for which the Marshall–Palmer $R(Z)$ relation underestimates the 1-h rain depth by a factor of 3. A dense network of 42 gauges was used to determine the rainfall over a 40 km × 50 km test area in the Little Washita River basin. To find the reason for the failure of the conventional algorithm, we have analyzed the contrasting case of another squall line (9 June 1993) for which the Marshall–Palmer relation works well.

The joint analysis of the reflectivity factor Z, the specific differential phase K_{DP}, and the differential reflectivity Z_{DR}, together with the vertical structure of the storms, leads us to hypothesize that the cause of the 300% error in the $R(Z)$ estimates is in the drop size distributions. It is very likely that in the February squall line rainfall was composed of drops within a narrow interval of diameters between 1 and 2 mm, whereas in the June storm the DSD had a broader spectrum and was close to the Marshall–Palmer distribution. Narrow DSD in the winter case could originate from nearly monodisperse graupel aloft that melted in the height interval between 2.5 and 1.0 km above the ground. Therefore, we hypothesize that equilibrium DSD has not been established and the shape of DSD near the ground was determined primarily by the size distribution of graupel aloft. Because the June storm had small hail, its DSD could not have reached equilibrium either. Nevertheless, the broader spectrum of hail sizes might have created a significant number of drops with large sizes so that the DSD was close to the Marshall–Palmer distribution.

Rain depths estimated from K_{DP} are in very good agreement with actual accumulations measured by gauges in both cases. This proves that the $R(K_{DP})$ relation is more robust and much less sensitive to DSD variations.

Acknowledgments. We are grateful to Mr. G. Heathman from the U.S. Department of Agriculture for providing rain accumulation charts for the network in the Little Washita River Basin. Dr. R. J. Doviak reviewed the manuscript, and Joan O'Bannon drafted Figs. 1 and 5. In his review Dr. R. Carbone brought to the authors' attention significant points and references that have enhanced the manuscript. An anonymous reviewer made helpful suggestions, for which we are grateful.

REFERENCES

Balakrishnan, N., and D. S. Zrnić, 1990: Estimation of rain and hail rates in mixed-phase precipitation. *J. Atmos. Sci.*, **47,** 565–583.

Bringi, V. N., V. Chandrasekar, N. Balakrishnan, and D. S. Zrnić, 1990: An examination of propagation effects on radar measurements at microwave frequencies. *J. Atmos. Oceanic Technol.*, **7,** 829–840.

——, D. A. Burrows, and S. N. Menon, 1991: Multiparameter radar and aircraft study of raindrop spectral evolution in warm-based clouds. *J. Appl. Meteor.*, **30,** 853–880.

Carbone, R. E., 1985: Comments on "Functional fits to some observed drop size distributions and parameterization of rain." *J. Atmos. Sci.*, **42,** 1346–1347.

——, and L. D. Nelson, 1978: The evolution of raindrop spectra in warm-based convective storms as observed and numerically modeled. *J. Atmos. Sci.*, **35,** 2302–2314.

Dingle, A. N., and K. R. Hardy, 1962: The description of rain by means of sequential raindrop-size distributions. *Quart. J. Roy. Meteor. Soc.*, **88,** 301–314.

Hu, Z., and R. C. Srivastava, 1995: Evolution of raindrop size distribution by coalescence, breakup, and evaporation: Theory and observations. *J. Atmos. Sci.*, **52,** 1761–1783.

Jameson, A. R., 1983: Microphysical interpretation of multi-parameter radar measurements in rain. Part I: Interpretation of polarization measurements and estimation of raindrop shapes. *J. Atmos. Sci.*, **40,** 1792–1802.

——, 1992: The effect of temperature on attenuation-correction schemes in rain using polarization propagation differential phase shift. *J. Appl. Meteor.*, **31,** 1106–1118.

National Climatic Data Center, 1994: *Storm Data.* Vol. 36, No. 2, NOAA, 42 pp.

Pruppacher, H. R., and R. L. Pitter, 1971: A semi-empirical determination of the shape of cloud and rain drops. *J. Atmos. Sci.*, **28,** 86–94.

Rosenfeld, D., E. Amitai, and D. B. Wolff, 1995: Classification of rain regimes by the three-dimensional properties of reflectivity fields. *J. Appl. Meteor.*, **34,** 198–211.

Ryzhkov, A. V., and D. S. Zrnić, 1995a: Comparison of dual-polarization radar estimators of rain. *J. Atmos. Oceanic Technol.*, **12,** 249–256.

——, and ——, 1995b: Precipitation and attenuation measurements at a 10-cm wavelength. *J. Appl. Meteor.*, **34,** 2121–2134.

Sachidananda, M., and D. S. Zrnić, 1987: Rain rate estimated form differential polarization measurements. *J. Atmos. Oceanic Technol.*, **4,** 588–598.

Srivastava, R. C., 1971: Size distribution of raindrops generated by their breakup and coalescence. *J. Atmos. Sci.*, **28,** 410–415.

Waldvogel, A., B. Federer, and P. Grimm, 1979: Criteria for the detection of hail cells. *J. Appl. Meteor.*, **18,** 1521–1525.

Wills, P. T., 1984: Functional fits to some observed drop size distributions and parameterization of rain. *J. Atmos. Sci.*, **41,** 1648–1661.

——, 1985: Reply. *J. Atmos. Sci.*, **42,** 1349–1350.

Witt, A., and S. P. Nelson, 1991: The use of single-Doppler radar for estimating maximum hailstone size. *J. Appl. Meteor.*, **30,** 425–431.

Zrnić, D. S., and A. V. Ryzhkov, 1996: Advantages of rain measurements using specific differential phase. *J. Atmos. Oceanic Technol.*, **13,** 454–464.